Search for the admixture of heavy neutrinos in the recoil spectra of ^{37}Ar decay

M. M. Hindi,[1] Recep Avci,[2] A. H. Hussein,[3] R. L. Kozub,[1] P. Miočinović,[1,*] and Lin Zhu[2,†]
[1]*Department of Physics, Tennessee Technological University, Cookeville, Tennessee 38505*
[2]*Department of Physics, Montana State University, Bozeman, Montana 59717*
[3]*Physics Program, University of Northern British Columbia, Prince George, British Columbia, Canada V2N 4Z9*
(Received 9 March 1998)

Neutrino-induced recoil spectra of ^{37}Cl ions produced in the electron capture (EC) decay of ^{37}Ar were measured and searched for the presence of massive neutrinos admixed to the dominant electron neutrino. Fractions of a monolayer of ^{37}Ar were physisorbed on Au and on several underlayers of ^{40}Ar adsorbed on both Au and graphite substrates cooled to $\leqslant 20$ K under ultrahigh vacuum conditions. Time-of-flight spectra of the recoiling ions were recorded in coincidence with x rays and Auger electrons emitted following the EC decay. By searching these spectra for peaks with energies between 7.6 eV and 3.6 eV upper limits were placed on the mixing probability of the electron neutrino with heavy neutrinos in the 370–640 keV mass range. These limits vary from 1 to 4 %, at the 90% confidence level. [S0556-2813(98)03810-2]

PACS number(s): 14.60.Pq, 23.40.−s

I. INTRODUCTION

Despite the passage of 68 years since its introduction by Pauli in 1930 [1] and over 40 years since its detection by Reines and Cowan in 1953 [2], one of the most fundamental properties of the neutrino, namely its mass, remains unknown. A nonzero neutrino mass could have profound implications for particle physics, astrophysics, and cosmology [3]. In particle physics the existence of neutrino mass could require the extension of the standard model and the introduction of new couplings and possibly new particles [3]. In astrophysics nonzero neutrino mass could help solve the solar neutrino problem and explain how supernovae explode [3]. In cosmology a neutrino mass in the few eV range could solve the (hot) dark matter problem and provide the mass necessary for closing the universe [3]. Reflecting this profundity, a substantial amount of experimental effort has been, and continues to be, directed at attempts to determine neutrino masses (the Review of Particle Physics [4] cites over 300 references under the heading ''Massive neutrinos and lepton mixing''). Yet, despite this substantial effort, only upper limits exist on the masses of the three neutrino flavors: 5–10 eV for ν_e [at 90% confidence level (C.L.)], 170 keV for ν_μ (at 90% C.L.), and 24 MeV for ν_τ (at 95% C.L.).[1] In this article we report a search for neutrinos with mass in the few hundred keV range. A tau neutrino in this mass range is viable and could have important cosmological consequences [5].

If neutrinos have mass then it is possible for the different neutrino flavors to mix. Such an admixture would exhibit itself in the kinematics of weak two-body and three-body decays in which the neutrino is one of the final products. The spectra of the accompanying particles in these decays would feature an extra peak (in the case of two-body decays) or a kink (in the case of three-body decays) the location of which will depend on the mass of the admixed neutrino and the strength of which will depend on the mixing angle. In the experiments reported herein, the spectrum of recoil velocities of the ^{37}Cl atom produced in the two-body electron capture (EC) decay of ^{37}Ar, $^{37}\mathrm{Ar}\rightarrow{}^{37}\mathrm{Cl}+\nu$, was measured. For an isolated ^{37}Ar atom energy and momentum conservation dictate that the recoil energy be 9.54 eV, if a neutrino with a negligible mass (ν_e) is emitted.[2] If a neutrino with mass m_ν is emitted in a certain fraction of the decays then the recoil energy of that fraction will be shifted down by $\Delta E = 9.54 \times (m_\nu/Q)^2$ eV, where Q is the decay energy [$=(814 - E_B)$ keV, with E_B being the excitation energy of the hole left in the daughter ^{37}Cl atom; for a K hole $E_B = 2.833$ keV, for an L_1 hole $E_B = 0.270$ keV [7]]. The recoil velocity was measured by recording the time-of-flight of the recoiling ions in coincidence with x rays and Auger electrons produced when the atomic hole in the ^{37}Cl is filled. The ^{37}Ar source was physisorbed on a cold substrate ($T \approx 20$ K) under ultrahigh vacuum (UHV) conditions.

The recoil velocity spectrum from gaseous ^{37}Ar was first measured in 1952 by Rodeback and Allen [8], using the time-of-flight technique. Their spectrum is too broad (due to the large spatial extension of the source region and to recoil from Auger electrons) and the statistics too poor, however, to be useful for a massive neutrino search. Singles spectra were measured by Kofoed-Hansen using crossed electric and magnetic fields [9] and by Snell and Pleasonton [10] using a

*Present address: Physics Department, University of California, Berkeley, CA 94720.

†Present address: Tosoh SMD Inc., Grove City, OH 43123.

[1]A measurement reporting a positive mass by Athanassopoulos *et al.* [36], has yet to be confirmed. See also Hill [37].

[2]There are two second order electron capture decay processes which result in a continuum of recoil energies. These are electron shakeoff accompanying electron capture and internal bremsstrahlung (IB) accompanying electron capture. The measured probability of double K-shell ionization per K capture in ^{37}Ar is $(3.7 \pm 0.9) \times 10^{-4}$ [38]. and the measured IB intensity per K capture is $(5.2 \pm 1.3) \times 10^{-4}$ [6]. The contributions of these processes to the recoil spectrum are therefore negligibly small.

magnetic spectrometer. The dominant source of broadening in these singles spectra is the recoil from the K Auger electrons that accompany about 80% of the decays, leading to a broadening of about 25% in the energy, and thermal broadening, which leads to a spread of about 18% in the energy. Kofoed-Hansen does not present differential spectra while Snell and Pleasonton show only the region of the main recoil peak; hence it is not possible to deduce limits on the mixing of massive neutrinos from these earlier papers.

Recoil following the electron capture decay of solid sources of ^{7}Be was also observed a long time ago [11–13], but the reported spectra are too broad to be useful for massive neutrino searches. The broadening in these spectra is partly due to the difficulty of achieving sub monolayer sources and to the relatively poor vacuum conditions available at the time (at the reported pressure of about 5×10^{-7} Torr [13] it would take only about 2 s to form a monolayer of the residual gases on top of the source, if the sticking coefficient were 1.0).

The method of using the recoil spectrum produced by lepton capture to search for massive neutrinos has been employed once before, by Deutsch *et al.* [14]. These authors analyzed an existing triton recoil spectrum produced following the muon capture reaction $\mu^{-}+{}^{3}\mathrm{He}\rightarrow\nu_{\mu}+{}^{3}\mathrm{H}$ to place limits, at the percent level, on the admixture of the muon neutrino to neutrinos with mass between 60 and 72 MeV.

There have been two other searches for the admixture of the electron neutrino with a heavy neutrino in a mass range that overlaps the mass range covered by the present work. Schreckenbach *et al.* [15] searched for a heavy neutrino in the mass range 30 to 460 keV by looking for kinks in the β^{+} spectrum of ^{64}Cu. The lowest limit they obtained was 3.5×10^{-3} at a neutrino mass of 350 keV. Deutsch *et al.* [16] searched for a heavy neutrino in the mass range 0.4 to 2.8 MeV by looking for kinks in the β^{-} spectrum of ^{20}F. The lowest limit they obtained was 1.7×10^{-3} at a neutrino mass of ≈1.4 MeV.

By adsorbing the ^{37}Ar source onto a cold (20 K) surface and detecting the K Auger electrons (or x rays) in coincidence with the recoiling ions, we had hoped to reduce substantially the contributions to broadening present in previous recoil measurements: (1) the localization of the source in an area of a few mm^2 would reduce the variation of flight path present in a gaseous source experiment, while at the same time increasing substantially the source strength. For example, the number of ^{37}Ar atoms in a monolayer of 1 mm^2 area is about 20 times that in a volume of 1 cm^3, at a pressure of 10^{-5} Torr and a temperature of 300 K (conditions similar to those of the experiment by Rodeback and Allen [8]). (2) At 20 K the thermal broadening is about 5% (in energy), compared to 18% at 300 K. (3) The detection of the K Auger electron reduces the broadening due to its recoil from 25% (for an undetected K Auger) to about 3% (for the geometry employed in this work; see below). (4) The vacuum employed in the current work ($\sim2\times10^{-10}$ Torr) is about three orders of magnitude lower than that employed in the early recoil studies with ^{7}Be [11–13], leading to correspondingly longer times before the formation of an overlayer of residual gases. With these improvements, we hoped to achieve sensitivities to the admixture of massive neutrinos comparable to, or lower than those achieved by the previous works of Schreckenbach *et al.* [15] and Deutsch *et al.* [16], in this mass region (400–800 keV).

Of course, a solid source has the disadvantage of a possibly large and complex interaction between the recoiling ion and the substrate, and with neighboring atoms. Molecular dynamics calculations by Glikman [17] on the desorption of radioactive palladium atoms from a palladium crystal indicated that the broadening due to such interactions is small if the recoiling atom is detected in a narrow angular range about the normal to the crystal. Similar calculations by our group (see below) for ^{37}Ar in an ^{40}Ar crystal and on top of a gold substrate indicated that the broadening would be relatively small. Of course, it remained to be seen whether the idealizations used in the calculations could be reproduced in the laboratory and whether the calculations ignored some potentially important interactions. Given the importance of the question of neutrino mass and the relatively low cost of this experiment, compared to other experiments searching for neutrino mass, we decided it is best to find out the answer by actually performing the experiment.

II. EXPERIMENTAL PROCEDURE

A. Source preparation

The ^{37}Ar source was produced via the $^{40}\mathrm{Ca}(n,\alpha)^{37}\mathrm{Ar}$ reaction. Pure Ca metal (99.99% elemental purity), in the form of crystalline dendritic pieces, ampouled under argon to prevent oxidation, was purchased from Johnson Matthey, Alfa Aesar. About 0.5 g of the Ca metal was encapsulated in a quartz tube. The Ca was outgased by heating it while pumping down the quartz tube with a turbomolecular pump. The quartz tube was sealed with a H_2/O_2 torch when the pressure dropped below 10^{-6} Torr. The sample was irradiated for six days at Brookhaven National Laboratory's High Flux Beam Reactor (HFBR) producing about 40 mCi of ^{37}Ar.

The ^{37}Ar was released from the Ca into a holding high vacuum chamber using the following procedure. The quartz tube containing the irradiated Ca was placed inside a larger quartz tube which was coupled to the holding chamber via a valve. The holding chamber and the quartz tube were baked at a temperature of 210 °C for 15 h while pumping with a turbomolecular pump. After cooling down for 7 h and reaching a pressure of 2.5×10^{-8} Torr the pumping was stopped; with the pumping halted the base pressure in the chamber reached 7.4×10^{-7} Torr. The quartz tubes were then heated radiatively in an annular electric oven to a temperature of 1000 °C and let stand at this temperature for about 10 min. At that point the Ca is melted completely (the melting point of Ca is 840 °C, that of quartz is 1700 °C) and the trapped ^{37}Ar (and ^{4}He) is released from the Ca metal into the still-sealed quartz tube. What releases the ^{37}Ar from the sealed quartz tube into the holding chamber is a fortuitous chemical reaction between the Ca and the inner surface of the inner quartz tube (SiO_2). Upon cooling down to a temperature of about 350 °C the bonded compound, presumably having a different thermal expansion coefficient from the outer quartz surface, cracks the inner quartz tube and releases the trapped gases into the outer quartz tube and the holding chamber. One indicator of the release is a jump in the pressure in the holding chamber from 6.0×10^{-5} to 5.4×10^{-4} Torr (with the quartz at 350 °C).

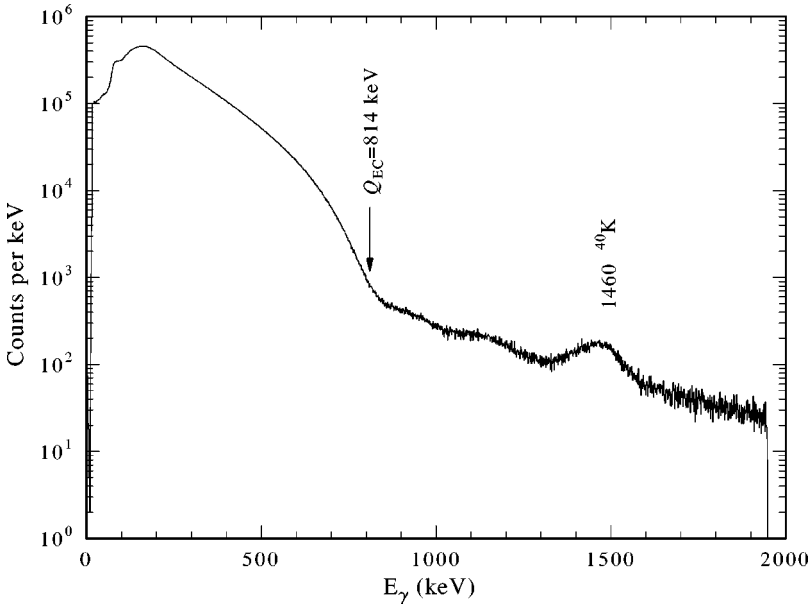

FIG. 1. γ-ray spectrum of the ^{37}Ar source adsorbed on zeolite. The spectrum was measured with a NaI detector. The γ-ray energy is in keV.

After allowing the quartz to cool down to room temperature, the released ^{37}Ar was trapped in the holding chamber by dipping a ''U'' tube filled with zeolite in a vessel containing liquid nitrogen (LN_2). The adsorption of the ^{37}Ar onto the zeolite was monitored by measuring the internal bremsstrahlung (IB) yield accompanying the EC decay of ^{37}Ar [6] with a NaI detector. The 5.7 cm diameter $\times$6.8 cm height NaI detector was Pb shielded so it would mainly see radiation from the ''U'' tube. Initially, when the activity of the ^{37}Ar was about 40 mCi, the IB count rate was about 3.4×10^4 counts per second. After adsorption of the ^{37}Ar onto the zeolite the valve separating the quartz tubing from the chamber was closed and the Ca and quartz tubing were removed from the vicinity of the experimental setup.

The radiopurity of the adsorbed gas is demonstrated in Fig. 1, which shows the spectrum of γ-ray energies recorded by the NaI detector. Since ^{37}Ar decays by a ground-state to ground-state transition, no γ-ray lines are expected in the spectrum. The dominant feature of the spectrum is the continuous IB radiation which has an end-point energy of 814 keV (the Q_{EC} value of the ^{37}Ar decay). Otherwise, the most prominent line is the 1460-keV ^{40}K line due to room background. Since the IB intensity per K capture in ^{37}Ar is known to be $(5.2\pm1.3)\times10^{-4}$ [6], we can deduce from the spectrum shown Fig. 1 the fraction of radioactive contaminants, if any, in the Ar source. Specifically, we have searched for ^{42}Ar by looking for the 1525-keV line which would arise from its decay chain. We can place an upper limit on the decay rate of ^{42}Ar of 10^{-6} of the ^{37}Ar decay rate. The other long lived Ar isotope which could conceivably be present is ^{39}Ar ($t_{1/2}=269$ yr) produced via the ^{42}Ca(n,α) reaction. There are no γ-ray lines associated with its decay and hence its presence cannot be deduced from the spectrum shown in Fig. 1; however, based on the natural abundance of ^{42}Ca (0.65%), and the Q values of the reactions [$Q=0.34$ MeV for ^{42}Ca(n,α) and $Q=1.75$ MeV for ^{40}Ca(n,α)] we estimate an initial activity of ^{39}Ar that is ≈0.4–2.3×10^{-6} of the ^{37}Ar activity. The procedure for introducing the ^{37}Ar into the ultrahigh vacuum chamber (UHV) that is used for the recoil measurements is described below.

B. Gas cleaning and dosing

Figure 2 shows a schematic representation of the experimental system. One component of the system is the holding chamber for the ^{37}Ar gas. Another is the UHV chamber housing the cooled sample upon which the ^{37}Ar is adsorbed and the detectors used in the recoil measurement. Not shown are a 130 l/s ion pump used for pumping the UHV chamber, and a He cryopump which cools the sample upon which the ^{37}Ar is adsorbed down to 15–20 K. The ^{37}Ar is dosed onto the sample using a doser (described below) that is connected to the holding chamber via a leak valve. Prior to dosing onto the sample the ^{37}Ar is ''cleaned'' in two ways. First, four wires made of a Ta-Ti alloy[3] (75% Ta and 25% Ti) in the holding chamber are heated to a temperature of $\geqslant2000\,^\circ$C by passing a current of 3.5 A in each wire. The heating evaporates and deposits a thin film of Ti on the walls of the holding chamber. This thin Ti film acts as a getter for most of the residual gases in the holding chamber (but not for Ar). The film maintains its pumping speed for about 24 h, after which a fresh film is deposited. Second, the ''U'' tube containing the zeolite is dipped into a LN_2 cup, thus freezing most of the residual gases (including the ^{37}Ar) onto the zeolite. The complete adsorption of the ^{37}Ar onto the zeolite is indicated by an increase and then a leveling of the IB count rate monitored by the NaI detector. The LN_2 is then allowed to evaporate and the ''U'' tube warm up until its temperature is about $-140\,^\circ$C, at which point the ^{37}Ar begins to be released from the zeolite. This release is evidenced by a decrease in the IB count rate recorded in the NaI detector. At that point the leak valve is opened and the ^{37}Ar dosed onto the sample via the doser.

The leak valve is connected with a Teflon tube to an opening in a stainless steel block (not shown in Fig. 2) that is mounted on a fixed frame within the UHV chamber. The sample could be brought to within a fraction of a mm in front of the opening while dosing. The diameter of the opening in

[3]Obtained from Getters Corporation of America, Cleveland, Ohio.

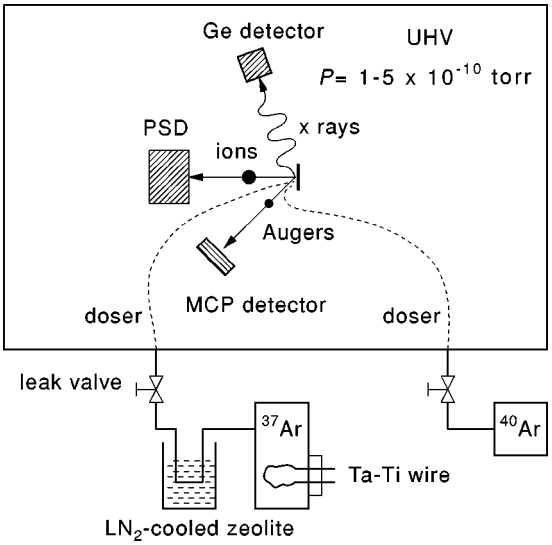

FIG. 2. Schematic illustration of the experimental setup.

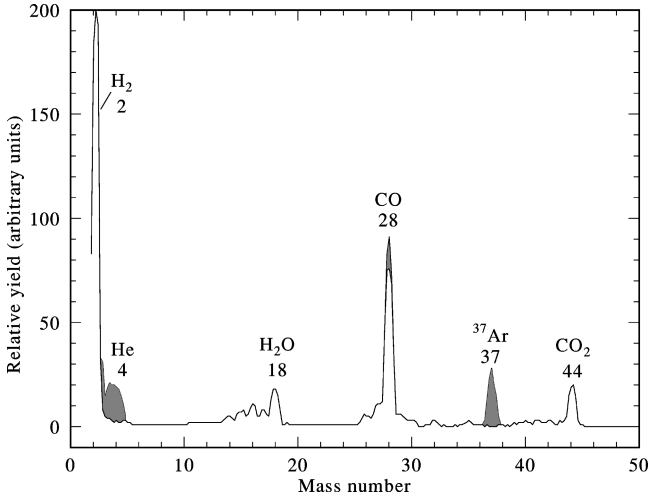

FIG. 3. Overlaid residual gas analyzer (RGA) mass spectra taken before and after opening the ^{37}Ar leak valve. The shaded area shows the excess yield with the ^{37}Ar leak valve open.

the block is 2.10 mm. The arrangement allows the ^{37}Ar gas to be adsorbed just on the sample, within an area of diameter comparable to that of the doser. The stainless steel block had another opening, with a diameter of 5.08 mm, above the ^{37}Ar doser. This larger opening was connected, again with a Teflon tube, to another leak valve through which ^{40}Ar could be dosed onto the sample (Fig. 2). When it was desired to use ^{40}Ar as a substrate, the sample would be brought in front of the larger opening, the ^{40}Ar dosed, then lowered by an amount equal to the distance between the centers and then the ^{37}Ar dosed. The sample was then raised so that the detectors had a clear geometrical path to the ^{37}Ar adsorbate.

The cleanness of the ^{37}Ar gas introduced into the UHV chamber is illustrated in Fig. 3, which shows a residual gas mass spectrum taken before the ^{37}Ar leak valve is opened, overlaid with a spectrum taken with the leak valve open (and with the sample warm). (The hatched areas in the figure show the excess yield with the leak valve open.) The background spectrum was taken at a base pressure of 1.5×10^{-9} Torr; the spectrum with the leak valve open was taken at a pressure of 3.0×10^{-9} Torr. The spectrum with the leak valve open shows an excess of mass 37 (^{37}Ar), mass 4 [^{4}He from α's produced in the ^{40}Ca$(n,\alpha)^{37}$Ar reaction], as well as a slight increases in masses 2 (H_2), and 28 (CO). Since H_2 and He do not get adsorbed onto the sample surface at our working temperature of about 20 K, their presence does not pose a problem. The slight excess of CO, though undesirable, is a small fraction of the CO already in the UHV system.

C. Graphite and Gold substrates

Two samples were used as cold substrates in the experiments: a graphite sample and a gold-coated Si sample. The graphite was a high grade pyrolitic graphite (HPG) sample of 12×10 mm^2 area and 2 mm thickness. The freshly cleaved HPG was examined by using a scanning tunneling microscope in air; this revealed an atomically flat surface. The HPG was cleaved again from both sides just before being put inside the UHV chamber.

Good thermal contact between the graphite substrate and the cold finger was maintained by a bridge machined from ultrahigh purity (99.999%) copper and a layer of indium between the copper and the HPG. The temperature was measured with a gold (with 0.07% Fe) vs Chromel thermocouple attached to the copper bridge, near the sample.

The gold-coated Si sample was manufactured at the nanofabrication facility of Cornell University. A 250 nm gold film was deposited on a large Si wafer. A sample with a size comparable to that of the graphite sample was cut out of the wafer and mounted on the Cu mounting bridge described above. Analysis of the gold surface with an atomic force microscope revealed islands, roughly circular in shape, with diameters ranging from 30 to 60 nm, and with heights varying from 6 to 10 nm.

D. Detectors

The UHV system housed three detectors (Fig. 2): an UHV-compatible germanium detector[4] to detect K x rays produced in filling the hole vacated by K-electron capture, a microchannel plate detector (MCP) to detect Auger electrons deexciting the ^{37}Cl atom, and another MCP detector to detect the recoiling ^{37}Cl ions. The x-ray detector is a high purity planar Ge crystal, 11.3 mm in diameter (100 mm^2 area) and 10 mm deep. The crystal is 5 mm away from an 8 μm thick Be window. It is a retractable detector equipped with a slide table, bellows and an UHV gate valve. In our current setup, the closest distance that the window can be brought to the sample is about 1.6 cm, leading to a maximum geometrical efficiency of about 1.7% (of 4π). The measured overall efficiency for runs using the gold sample was 0.44%. This is (37 ± 3)% of the expected efficiency for a point source. This reduction is probably partly due to absorption of the x rays within the sample. The x-ray detector was at an angle of 74° from the normal to the sample, and subtended a half-cone

[4]Canberra Model No. 7905-BWR, Canberra Industries, Meriden, Connecticut.

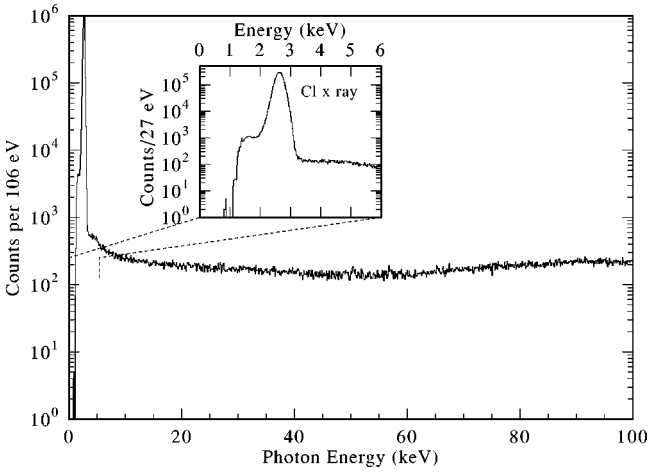

FIG. 4. A sample γ-ray spectrum recorded with the Ge detector. The inset shows the profile of Cl x rays that follow the EC decay of the ^{37}Ar source.

angle of 12.7°. A substantial portion of the x rays emitted at small angles from the surface could have been scattered or absorbed by the islands seen on the Au surface. For runs using the graphite substrate, the effeciency was 0.84%, which is $(60\pm7)\%$ of the expected efficiency. The detector subtended a half cone angle of 14.4° in that case, and again it may be that a portion of the x rays emitted nearly parallel to the surface were absorbed by small structures on the surface.

Figure 4 shows a sample spectrum recorded with the x ray detector. The spectrum, which shows only Cl x rays and a continuum dominated by room background and (to a much lesser extent) IB from the EC decay of ^{37}Ar, confirms the radiopurity of the adsorbed sample. The inset shows the measured profile of the Cl x-ray peak. The FWHM is 310 eV, which is substantially worse than the specified resolution of 150 eV (at 5.9 keV); this degradation is primarily due to the use of a 3 μs shaping time on the amplifier, instead of the usual 12 μs required for optimum resolution with this detector. Since the present measurements do not require the higher resolution and it was simpler to setup the electronics for the 3 μs pulses, we opted to work at that setting.

The Augers MCP detector consisted of two stacked microchannel plate detectors each 2.5 cm in diameter. The assembly was at an angle of 60° from the normal to the sample, at a distance of about 8 cm from it. Three screens, each with a transmission of 81%, were placed in front of the MCPs. The first and last screens were grounded; a negative bias V applied to the middle screen restricted the MCP to detecting electrons with energy $E \geqslant eV/\sin^2\theta$, where θ is the angle of incidence of the electron on the screen ($\theta=90°$ being normal to the screen). To detect both L and K Auger electrons a retarding voltage of 100 V was usually applied to the middle screen ($E_{LMM}\approx175$ eV, $E_{KLL}=2400$ eV, $E_{KLM}=2600$ eV), while to detect only K Augers a retarding voltage of 300 V was typically used [18].

The ion MCP detector also consisted of two stacked microchannel plate detectors with a 2.5 cm diameter. The three screens in front of the microchannel plate (each with 81% transmission) were separated by 1.6 mm, and the distance between the last screen and the first MCP was 5.1 mm. The front of the MCP was at a bias of -2.8 kV relative to the (grounded) last screen. Thus the slow (≈10 eV) positively charged ions were accelerated over the last 0.5 cm to an energy of $2.8q$ keV, where q is the charge state of the ion, before impinging on the MCP. Previous studies [19] have shown that the MCP detection efficiency for Ar^+ saturates at an energy of 3 keV. A 100 kΩ resistive anode encoder (RAE) plate behind the last MCP gave the two-dimensional (2D) position of the impinging ion. This position could be used to correct for the variation of flight path over the angular opening of the detector. Unfortunately, a loss of signal from one of the corners of the RAE prevented us from making this correction for all of the collected data.

The ion detector was mounted on a linear motion feed through located at 0° with respect to the sample. The detector could be moved from about 2.5 to about 17.5 cm from the sample, with a precision of 0.01 mm. To determine the absolute velocity of the recoils (and hence to deduce the effective flight path), the change of flight time was measured for a known change of detector distance (usually about 1.500–2.000 cm). The effective flight paths employed in the neutrino mass search varied from a low of 3.17 ± 0.05 cm (for those runs in which the 2D position information was available), to 4.00 ± 0.05 cm (runs for which the position information was not known).

E. Data acquisition

The linear and fast signals from the detectors were processed using standard NIM electronic modules and digitized in a CAMAC crate interfaced to a PC running a locally written DOS-based multiparameter data acquisition system. The digitized signals were collected event by event and written on magnetic tape for later analysis. The collected signals were the following: (1) the energy registered in the x-ray detector, digitized in an 8k analog-to-digital converter (ADC); this signal was collected for every event. (2) The four corner signals from the RAE, each digitized in an 8k ADC; these were typically collected only when the ion detector was in coincidence with another detector. (3) The time of flight of the ion, measured with a time-to-amplitude converter (TAC) and digitized in an 8k ADC. The TAC was started on either the x-ray or the Auger detector (their fast signals were OR'ed), and stopped on the ion detector. The TAC signal was collected only for coincidence events. The TAC was set to 20 μs full scale. (4) The time difference between any pair of detectors, digitized in an eight channel time-to-digital converter (TDC). The TDC was started on an OR of the fast signals of all the detectors and each detector had its own stop channel. The full scale on the TDC was 1 μs. (5) Logic signals to indicate which of the detectors fired. (6) Total singles counts registered by the ion and Auger MCPs, read every 2 s.

As mentioned above, runs were conducted using graphite and gold samples. Between the graphite and gold runs the UHV system was opened up and several improvements were made: (1) new ion pump elements were used, (2) the ^{40}Ar doser was installed, and (3) a more efficient sample heater was installed.

1. Runs with the graphite sample

Apart from a variety of calibration runs, all of the runs that were used to accumulate statistics for the massive neu-

trino search using the graphite sample were conducted by first adsorbing several layers of ^{40}Ar on the graphite and then adsorbing the radioactive ^{37}Ar on top of the ^{40}Ar. In a typical run 10 Langmuirs[5] (L) of ^{40}Ar were adsorbed on the graphite substrate by flooding the UHV chamber with ^{40}Ar at a pressure of 5×10^{-8} Torr for 200 s, with the ion pump off. After closing the ^{40}Ar valve and waiting (for a couple of minutes) for the pressure to drop to $\approx2\times10^{-9}$ Torr, the ion pump was turned on again. The ^{37}Ar was then dosed, again within a few minutes, by opening the leak valve to the ^{37}Ar chamber and monitoring the count rate in the x-ray detector. Dosing was usually stopped when the x-ray count rate reached ≈50 counts per second (cps), with the sample in the dosing position; this corresponded to a count rate of ≈100 cps, with the sample in the counting position. The corresponding activity of the ^{37}Ar source was 6.8 μCi. The number of atoms (1.10×10^{12}) corresponded to a coverage of 0.040 monolayers (ML), assuming the atoms covered an area of 3.5 mm^2 (the possibility that the ^{37}Ar atoms get ''clumped,'' i.e., form one or more layers over a much smaller area, has been considered and found to be highly unlikely; the relevant arguments are given in Sec. III). The corresponding count rate in the electron detector was ≈1400 cps, with a retarding voltage of 100 V, and the initial count rate in the ion detector was ≈1500 cps. Because of the adsorption of residual gases on top of the ^{37}Ar, the ion count rate decreased monotonically with time, reaching half its initial value in about 2 h. Because of this decrease, a typical dose was usually run for a few hours, after which the ^{40}Ar/^{37}Ar layers were desorbed by warming the graphite sample to a temperature of $\geqslant50$ K, and the above described procedure repeated for the next run. The desorption of the ^{37}Ar layer was indicated by a drop in the x-ray count rate to a few cps. The desorption of the ^{40}Ar multilayers was indicated by a rise in the pressure as the ^{40}Ar desorbed, followed by a drop in the pressure as the ^{40}Ar was pumped away. We have conducted time scans on mass 40 using the residual gas mass analyzer (RGA), and these also indicated that the ^{40}Ar multilayers had been essentially pumped away by the time the temperature reached about 50 K. It should be noted, however, that desorbing the first ^{40}Ar layer (i.e., the one on top of the graphite) requires a temperature of about 120 K, due to the tighter binding of Ar with graphite (compared to the binding of Ar with Ar).

2. Runs with the gold sample

With the gold sample, statistics for the massive neutrino search were collected using two types of runs: (1) with the ^{37}Ar dosed on top of the Au substrate directly and (2) with the ^{37}Ar dosed on top of several layers of ^{40}Ar which were first dosed on top of the Au. Since for the Au runs the ^{40}Ar doser had been installed, it was not necessary to flood the whole chamber with ^{40}Ar, nor to turn the ion pump off during the ^{40}Ar dose. Because the ^{40}Ar was dosed straight onto the sample, there was no pressure change to indicate the amount of ^{40}Ar coverage. Instead we relied on the time the ^{40}Ar leak valve was open. The required length of time was calibrated roughly by first dosing ^{37}Ar onto the Au sample, and then finding the time required to cover the ^{37}Ar with enough ^{40}Ar layers to reduce the recoil ion count rate to about 1/6 of its initial value. The number of layers needed to achieve such a reduction had been determined from similar runs conducted on top of the graphite, where the ^{40}Ar exposure was known from the pressure to be ≈10 L.

Because of the new ion pump elements, and the reduction in ^{40}Ar exposure, the vacuum was better for the Au runs than for the graphite runs. As a result, the time required for the ion count rate to drop to half its value was extended to about 4 h. A new heating filament just behind the sample allowed the ^{37}Ar and ^{40}Ar to be desorbed much more quickly (within 10 s) and without degrading the vacuum substantially, since the heating was quite localized.

The statistics used in the massive neutrino search presented herein were collected in 118 runs (i.e., 118 cycles of dosing and desorbing) over a period of 156 d. The same ^{37}Ar source was used for all of the runs.

III. DATA ANALYSIS AND RESULTS

Figure 5 shows sample time of flight spectra (TOF) taken on top of ^{40}Ar (with gold as the substrate for the ^{40}Ar), in coincidence with x rays [Fig. 5(a)] and with Auger electrons [Fig. 5(b)], and on top of gold [Figs. 5(c) and 5(d)]. The TOF spectra shown were all taken at a distance of 4.00 ± 0.05 cm. Figure 6 shows the same spectra, converted to energy scale, after subtracting the contribution of accidental coincidences. The broadening and the extra energy observed in the spectrum of recoils in coincidence with Augers, with ^{40}Ar as the substrate [open circles in Fig. 6(a)], are primarily due to inelastic charge exchange reactions with the ^{40}Ar bedding. The Auger cascade resulting from a K hole leads to charge states of $+2$ or higher, with charge state $+3$ being the predominant one [10,18]. Table I shows the ionization potentials for Cl and Ar, for various charge states. From the table it is clear that a Cl^{+q} ion, with $q\geqslant2$, can capture an electron from a neutral Ar, with a release of energy. When the K hole decays by x-ray emission, on the other hand, the final charge state is predominantly $+1$ and charge exchange, if it does occur, is endoergic. Even if charge exchange does occur for Cl^{+1}, the forward moving Cl will become neutral and will not be detected by the ion detector. A small fraction of the Cl ions that accompany the radiative decay of the K hole become doubly charged as a result of the double Auger (DA) decay of the $L_{2,3}$ hole created following $K\alpha_{1,2}$ x-ray emission. The probability of DA decay of the $L_{2,3}$ hole is $(9.3\pm0.3)\%$ [20]. Therefore that fraction of Cl ions accompanying x-ray emission may undergo an exoergic charge exchange reaction with the Ar substrate and still be detected.

Because of their very large widths, the spectra in coincidence with Augers, with ^{40}Ar as the substrate, were not used in the massive neutrino search. Therefore, from the spectra collected with ^{40}Ar as the substrate, only those in coincidence with x rays were searched for massive neutrinos, while for those spectra collected with Au as the substrate, both types of spectra (in coincidence with x rays and with Augers) were searched.

[5]One Langmuir is the exposure of a surface to 10^{-6} Torr s and represents one monolayer for a sticking coefficient of 1.

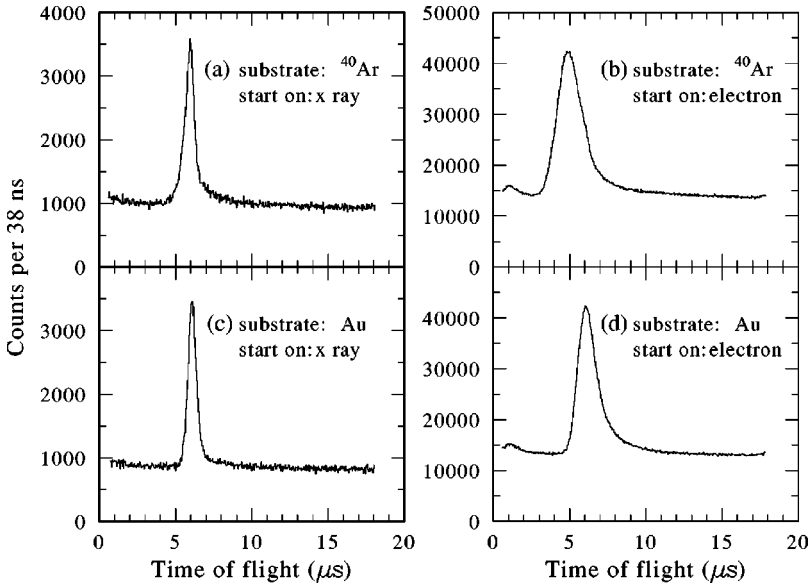

FIG. 5. Sample time of flight spectra of ^{37}Cl ions after EC decay of 0.06 ML ^{37}Ar (a) adsorbed on top of several ^{40}Ar layers on a gold substrate, in coincidence with Cl K x rays, (b) in coincidence with Cl L or K Auger electrons, (c) adsorbed directly on a gold substrate, in coincidence with x rays, and (d) in coincidence with Auger electrons.

Because there were variations (outside of statistical errors) in the position and width of the main peak in the TOF spectra obtained in different runs, the data from each run were examined individually and only data from runs in which the widths and centroids were close were added. The variation in width and centroid is possibly due to variations in the amount of residual gases adsorbed along with the ^{37}Ar on the substrate; the variation in the amount of residual gases is itself due to variations, from run to run, in the base pressures in the UHV chamber and in the ^{37}Ar holding chamber. Twelve spectra of the type shown in Fig. 5(b), comprising data from 62 runs (i.e., 62 different dosing plus desorption cycles), were each individually searched for a massive neutrino peak, as described below. The total counting time for these twelve spectra was 362 h and the total number of counts in the main peak is 1.7×10^6 counts. The recoil energy, averaged over the 12 spectra, is 8.02 eV, with a standard deviation (σ) of 0.66 eV. The average full width at half maximum (FWHM) is 3.53 eV with a σ of 0.19 eV. Similarly, twelve spectra of the type shown in Fig. 5(c) (the same 62 runs noted before, but for coincidences with x rays), having a total of 8.1×10^4 counts in the main peak, were searched for massive neutrinos. The average recoil energy was 8.42 eV with a σ of 0.23 eV, and the FWHM was 1.76 eV with a σ of 0.19 eV. Four spectra of the type shown in Fig. 5(a) (coincidences with x rays, with ^{40}Ar as the substrate), comprising data from 56 runs, were similarly fitted. The total counting time for these was 222 hours and the total number of counts in the main peak is 1.1×10^5 counts. About half of those counts came from spectra collected with the ^{40}Ar adsorbed on top of the graphite sample (rather than gold). The average recoil energy in these spectra is 8.89 eV, with a σ of 0.45 eV, and the average FWHM is 2.31 eV, with a σ of 0.26 eV. For comparison, the statistical uncertainty in determining the peak position (in all of the analyzed spectra) was only about 0.02 eV. The uncertainty in determining the flight distance results in an uncertainty of about

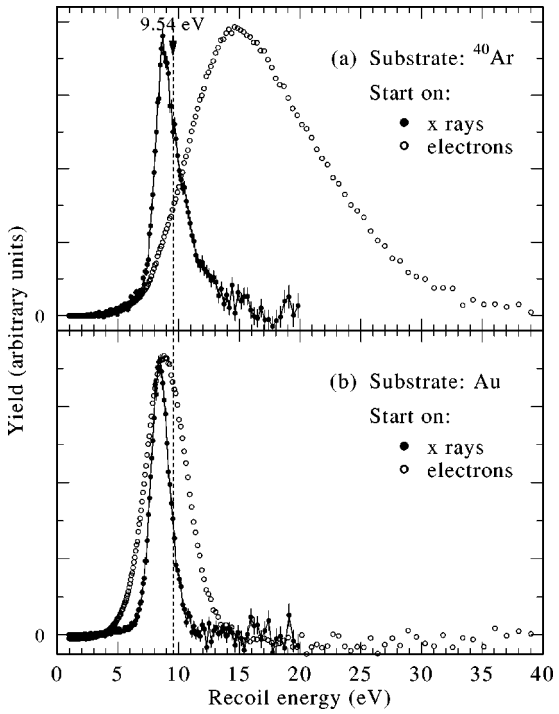

FIG. 6. Same spectra as in Fig. 5, converted to energy scale, after subtracting accidental coincidences. (a) Spectra taken with the ^{37}Ar adsorbed on top of several layers of ^{40}Ar, in coincidence with x rays (solid circles) and Auger electrons (open circles). (b) Spectra taken with the ^{37}Ar adsorbed on top of gold, in coincidence with x rays (solid circles) and Auger electrons (open circles). The dashed line at 9.54 eV indicates the expected recoil energy from a free ^{37}Ar atom.

TABLE I. Ionization potentials for Ar and Cl (eV) [39].

Charge	+1	+2	+3	+4
Cl	13.0	23.8	39.6	53.5
Ar	15.8	27.6	40.7	59.8

TABLE II. Statistics of coincidence spectra searched for massive neutrino.

	Electron-ion on Au	x-ray–ion on Au	x-ray–ion on ^{40}Ar
Number of spectra	12	12	4
Number of runs	62	62	56
Counting time (h)	362	362	222
Total counts	1.7×10^6	8.1×10^4	1.1×10^5
$E=$ Recoil energy (eV)	8.02	8.42	8.89
σ_E (eV)	0.66	0.12	0.45
$\Gamma=$ FWHM (eV)	3.53	1.76	2.31
σ_Γ (eV)	0.19	0.19	0.26

0.2 eV in the recoil energy. The statistics of these spectra are reproduced in Table II.

A. Monte Carlo simulation of the charge and energy distribution of recoils

1. Au substrate

In Fig. 6 the spectra are normalized to the same height, in order to illustrate the dependence of the width and energy of the recoils on the substrate and on the atomic decay channel. Another difference between the spectra, not apparent in Fig. 6, is that the fraction of ions detected in each spectrum is also different. With ^{40}Ar as the substrate we detect $(80\pm10)\%$ of the ions expected to be in coincidence with Auger electrons and $(38\pm4)\%$ of the ions expected to be in coincidence with x rays. With Au as the substrate we detect $(26\pm3)\%$ of the ions expected to be in coincidence with Auger electrons and $(17\pm2)\%$ of the ions expected to be in coincidence with x rays. The decrease in the detected fraction as the substrate changes from ^{40}Ar to Au is due, primarily, to neutralization of the recoiling ions by electron transfer from the Au substrate. [One does not expect the ^{40}Ar substrate to neutralize singly charged Cl; therefore, the detection of only $(38\pm4)\%$ of the Cl ions on top of ^{40}Ar for the x-ray channel is somewhat puzzling. We postulate that it is due to charge exchange with the small amount of residual gases, such as $CH_n(n\leqslant4)$, CO, CO_2, and H_2O, that get adsorbed along with the ^{37}Ar.]

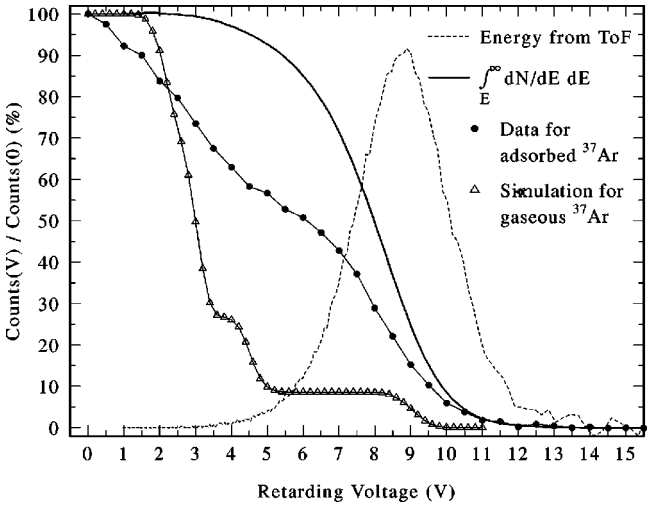

FIG. 7. A comparison between the measured retarding field spectrum of Cl ions recoiling from the decay of ^{37}Ar adsorbed on Au (solid circles) and that expected from gaseous ^{37}Ar (open triangles). The solid line gives the retarding spectrum that would be deduced from the TOF spectrum, if all the ions had charge $+1$ (solid line). The latter is obtained by integrating the energy spectrum that is obtained from the TOF (dashed line) from $E=V$ to $E_{\max}$.

Some limits on the charge state distribution of the recoiling ions can be obtained from the measurement of a retarding field spectrum: the count rate of ions as a function of a retarding potential V on the middle screen in front of the ion MCP detector. Figure 7 shows the retarding field spectrum measured for Cl ions recoiling from the decay of ^{37}Ar adsorbed on Au (solid circles). For comparison, a Monte Carlo simulation showing the retarding spectrum expected from a gaseous ^{37}Ar source (i.e., an idealized source without any backing) is also shown (open triangles). Details of the simulation are given below. As Table III shows, the charge state distribution obtained from the simulation agrees reasonably well with that measured by Snell and Pleasonton [10]. As can be seen in Fig. 7, the spectrum we measured differs substantially from the simulated spectrum, because the charge state distribution of ions recoiling from the surface is different from that of ions recoiling in the free gaseous state. In the gaseous state, $\geqslant90\%$ of the ions would have a charge state of $+2$ or higher; since the maximum energy of the ions is 12 eV, a retarding potential of 6 V would drop the count rate to $<10\%$ of that observed at 0 V (Fig. 7, open triangles). In contrast, the measured retarding spectrum shows a relative count rate of about 50% at 6 V, indicating that at least 50% of the ions recoiling from the Au surface have a

TABLE III. Relative intensities of the charge states of the ^{37}Cl ions (%).

	Gaseous ^{37}Ar		^{37}Ar adsorbed on Au	
Charge state	Expt. [a]	Monte Carlo	Expt. [b]	Monte Carlo
$+1$	6.2	8.5	53–63	69–89
$+2$	15.7	18.1	3–47	11–31
$+3$	39.2	43.1	<35	0–6
$+4$	26.7	21.6		
$+5$	10.0	7.3		
$+6$	1.8	0.8		
$+7$	0.4	0.0		

[a]Reference [10].
[b]This work.

charge state of $+1$. An *upper* limit on the fraction of charge state $+1$ can be deduced from the energy spectrum in coincidence with Auger electrons (the dashed line in Fig. 7), which should be very close to the singles energy spectrum. If all the ions had charge $+1$ then the retarding spectrum would simply be $\int_{E=eV}^{E_{\max}}(dN/dE)dE$, which is shown in Fig. 7 as the thick solid line. The count rate at $V=5.5$ V would then be about 90% of that at $V=0$ V. The observed yield at $V=5.5$ V is only 53%, indicating that at least 37% of the ions must have charge $+2$ or higher. From similar considerations we find the limits listed in column 4 of Table III for charge states 1^+–3^+.

In order to convert the area of a possible peak (due to the emission of a heavy neutrino) to a mixing fraction, one needs to know how the fraction of ions that escapes neutralization varies with energy. Qualitatively, one would expect a higher fraction of the low energy recoils produced by heavy neutrino emission to be neutralized, because of the longer time such recoils would spend in the vicinity of the neutralizing species (the Au substrate and/or the residual gases). As we point out below, it is possible, but extremely difficult, to determine this fraction experimentally. Instead, we have relied on a Monte Carlo (MC) simulation to calculate the fraction of Cl ions that escapes the Au substrate, as a function of recoil energy.

The two dominant mechanisms by which charge gets transferred from the Au substrate to the recoiling atom are Auger neutralization (AN) and resonant neutralization (RN). In AN a vacant orbital in the atom is filled by an electron from the substrate, with the difference in energy going to eject another electron from the metal. In RN a single electron is simply transferred from an orbital in the valence band of the metal to the empty orbital in the atom, where both orbitals have the same binding energy (hence the term resonant transfer).

The transition rates for AN and RN can be well approximated by a simple exponential dependence on the distance s of the ion from the surface [21,22]: $R(s)=A\exp(-as)$, where A and a are constants. Hagstrum [22] has shown that a most likely lies between 20 and 50 nm^{-1}. In the MC calculation we have considered values of a of 20, 35, and 50 nm^{-1}. For each value of a, the strength A was adjusted to reproduce the measured fraction of ions that was detected [$(26\pm3)\%$ for ions in coincidence with Auger electrons and $(17\pm2)\%$ for ions in coincidence with x rays]. For each fitted value of A, the MC simulation was repeated at ion energies of 3.0–8.5 eV, in steps of 0.5 eV, and the fraction of ions detected in coincidence with Auger electrons and with x rays was computed. The differences in the calculated fractions for the different values of a were $\leqslant 20\%$, with the largest differences occurring for the lowest energy ions.

In the MC calculation, the recoiling ion was assumed to interact with its image charge in the Au. Because the ion starts close to the surface, the classical Coulombic image potential for an ion of charge Z

$$\Phi_I(s)=-\frac{Z^2}{4s}$$

(in atomic units), which is valid for large distances s from the surface, is not valid in our case. Instead, we used the image potential derived by Echenique *et al.* [23] (in atomic units)

$$\Phi_I(s)=-\frac{Z^2\omega_s^2}{2}\int_0^\infty \frac{e^{-2ps}\,dp}{\omega_s^2+\alpha p+\beta p^2+p^4/4},$$

where ω_s is the surface-plasmon frequency, $\alpha=\sqrt{3/5}v_F\omega_s$, with v_F the Fermi velocity in the valence band, and β is a parameter ≈ 0.35 for Au [24]. The above potential reduces to the Coulombic potential for large s, but approaches a finite value for $s=0$. For Au $\hbar\omega_s=6.37$ eV and $v_F=1.39\times10^8$ cm/s [25].

The recoil induced by Auger-electron and x-ray emission was taken into account in the MC calculation. The lifetime and branching ratio for the Auger and radiative transitions were taken from Refs. [26–28]. In addition to single Auger transitions, we also allowed for the double Auger decay of the $L_{2,3}$ holes [20], but did not take into account the DA decay of the K hole [18]. Thermal broadening was taken into account by giving the ^{37}Ar an initial Maxwellian velocity distribution. However, at our substrate temperature (≈ 20 K), thermal effects are small compared to broadening from Auger recoil and variations in the image potential. The latter results from the differing charge states and the different distances from the surface at which the Cl develops its final charge.

Figure 8 compares samples of measured TOF spectra in coincidence with Auger electrons [Fig. 8(a)] and x rays [Fig. 8(b)] with the spectra obtained from a MC simulation. For this simulation $A=320$ fs^{-1}, $a=20$ nm^{-1}, and the initial position s_0 at the time of recoil was taken as 0.30 nm. While the agreement is not quantitative, the MC calculation does account for a fair share of the broadening in the spectra and for the differences observed between the Auger channel and the x-ray channel. It also accounts for the observed downward energy shift (due to the image potential) apparent in Fig. 6. The MC calculation also gives a fraction $F_1=72\%$ for charge 1 that is in rough agreement with that measured from the retarding voltage spectrum discussed above ($F_1 \leqslant 63\%$). (Column 5 of Table III lists the ranges of the charge fractions given by the MC calculation, for the range of values of the parameter a considered above.) The low energy peaks (long TOF) in the MC calculations are due to charge $+2$ ions. As mentioned above, in the x-ray channel charge $+2$ arises from the double Auger decay of the L hole. Clearly, the MC calculation does not quite account for the intensity of the observed tail, nor its shape, indicating that part of the broadening (and the tail) possibly comes, as speculated above, from interactions with residual gases adsorbed on the Au. In addition to relying on the MC calculation to get the fraction of ions escaping neutralization for the lower recoil energies which would accompany heavy neutrino emission, we used the MC calculation to account for the change in peak width and energy shift with the change in recoil energy.

2. ^{40}Ar substrate

In addition to the above MC calculation, we also performed extensive molecular-dynamics–MC calculations of

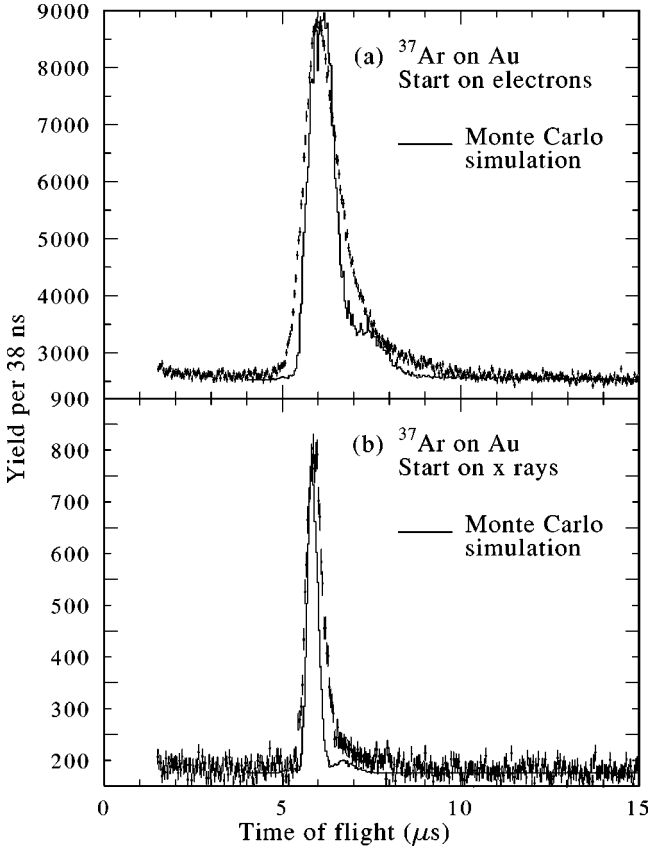

FIG. 8. Comparison between the measured time of flight spectra (data points with solid error bars) and a Monte Carlo simulation (solid line), for coincidences with Auger electrons (a) and x rays (b). The spectra are for ^{37}Ar adsorbed on gold.

the spectra of ions in coincidence with x rays, when the ^{37}Ar is adsorbed on ^{40}Ar. The simulation takes into account the thermal motion of the atoms, the Lennard-Jones type interactions between the atoms, and the induced dipole interaction between the desorbing ion and the crystal atoms. The potential parameters were taken from Ref. [29], the lattice constants from Ref. [25], and the polarizabilities from Ref. [30]. Figure 9 shows a comparison between a measured spectrum and the results of a molecular dynamics simulation for an initial single ^{37}Ar atom situated on top of 4 monolayers of ^{40}Ar (short-dashed line), and a simulation for an ^{37}Ar atom embedded in a completed topmost layer (long-dashed line). The secondary low energy peak in the simulated spectra arises from charge $+2$ ions produced following the DA decay of the $L_{2,3}$ hole. Inelastic charge exchange between such doubly charged Cl and the ^{40}Ar substrate was not taken into account in the simulation. The broadening of the peaks in the simulation is due primarily to the variation in the distance at which the monopole-dipole interaction between the recoiling Cl ion and the substrate is turned on. This variation in distance comes about from the spread in decay times about the 10 ns average lifetime (1 ns for the K hole $+9$ ns for the $L_{2,3}$ hole) during which the Cl atom is neutral. As can be seen from the figure, both simulations give peak widths (0.75 eV) which are less than half of the measured width. A simulation in which the number of ^{40}Ar atoms surrounding the ^{37}Ar atom was varied randomly also failed to reproduce the measured width. Here again, the most likely reason for the extra

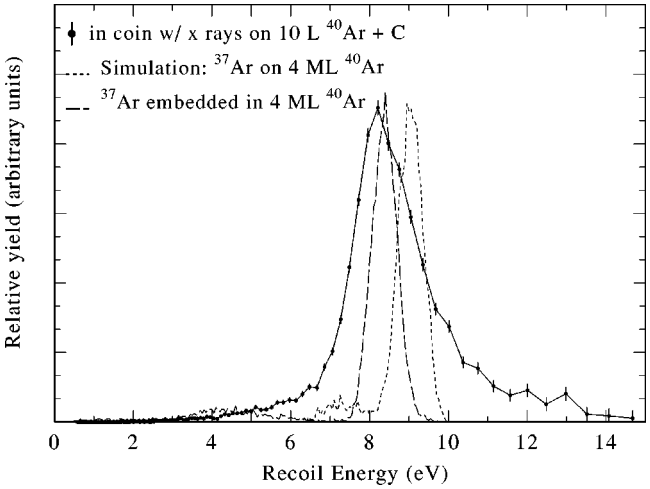

FIG. 9. Comparison between a measured energy spectrum for recoils from ^{37}Ar adsorbed on a film of 10L ^{40}Ar adsorbed on graphite (solid line with error bars) and a molecular-dynamics–MC simulation. The short-dash line shows the simulated spectrum for an isolated ^{37}Ar atom on top of 4 monolayers of ^{40}Ar; the long-dash line shows the simulated spectrum for ^{37}Ar embedded in the topmost layer of a four-layer film. The spectra are for coincidences with x rays.

broadening is the interaction of the recoiling Cl with residual gases adsorbed along with the ^{37}Ar. The polarizability of these gases is about double that of Ar. That the Cl interacts with atoms other than Ar is further indicated by the observed loss of ions. One would expect no loss of ions for an ^{40}Ar substrate, while the measured ion fraction in coincidence with x rays is only 38%. Therefore, in accounting for loss fractions and for broadening for spectra collected with ^{40}Ar as a substrate, we did not rely on this molecular dynamics calculation. Instead, we assumed that the neutralization rate is also given by $R=A\exp(-as)$, where, as in the Au case, A was adjusted to give the observed fraction (38%) at a recoil energy of 9.54 eV, and that A was used to predict the fraction at lower energies. We followed this procedure for the two limiting values of a considered above, and again the differences were $\leqslant 20\%$. For the width, we assumed that broadening is caused primarily by collisions with neighboring atoms and hence that $\Delta E/E$ is a function of scattering angle and mass of scattering species only, but not of the original energy.

We have considered the possibility that the ^{37}Ar atoms get ''clumped,'' i.e., form one or more layers over an area much smaller than that of the doser, and considered if such clumping might account for the larger than expected widths of the peaks and the reduction in the observed yield of the recoils. We offer the following reasoning to indicate that clumping probably does not happen on Au. Given the area of the doser it is of course very highly unlikely that the ^{37}Ar is deposited in a clump. In order for clumping to happen the atoms have to diffuse on the surface *after* being adsorbed, presumably because of the very weak induced-dipole induced-dipole attraction between the ^{37}Ar atoms. However, we believe the mobility of the ^{37}Ar along the surface (whether it is the Au surface, or the ^{40}Ar surface) is very small. The evidence we have for that is that the count rate in the x-ray detector remains very steady (within 1 or 2%) for

many hours, while the ion count rate decreases continuously, as the surface of the sample gets covered with residual gases. If the ^{37}Ar had great mobility on the surface, the ^{37}Ar would probably have spread out with time, since the attraction of Ar to the residual gases is stronger than that of Ar to Ar. The movement of the ^{37}Ar on the surface would have resulted in an observable change in the x-ray count rate. We had also conducted some test runs on graphite with a collimator in front of the sample. The collimator masked all of the sample except for a small circular area. Counts were observed only when the hole in the collimator was in front of the part of the sample that was dosed. Repeating the test at a later time convinced us that the ^{37}Ar stays stuck to the same spot for a long time.

For ^{37}Ar dosed onto ^{40}Ar we also considered the possibility that the ^{37}Ar is mixing with the ^{40}Ar (i.e., ''sinking'' into the ^{40}Ar layers), instead of just staying in the top layer. In that case one would have expected the broadening due to collisions with the ^{40}Ar on the way to the detector to affect the Cl–x-ray and Cl-Auger peaks in a similar way and hence to make the widths of the two peaks more similar than they are. As is clearly evident in Fig. 6(a), the widths of the two peaks are very different. Figure 6(a) also provides another evidence that such a mixing (or clumping) is not taking place: if a sizeable fraction of the ^{37}Ar was *underneath* the ^{40}Ar then one ought to have seen a reasonable number of $^{40}Ar^{+}$-Auger coincidences, the $^{40}Ar^{+}$ arising from $^{37}Cl^{+3}+{}^{40}Ar^{0}\rightarrow Cl^{+2}+{}^{40}Ar^{+1}$ scattering. Such $^{40}Ar^{+}$ scattered into the detector by the Cl would, in general, (except for head-on collisions) have less energy than the Cl and hence would contribute a low energy tail to the peak in coincidence with Augers. As Fig. 6(a) shows, that peak is only shifted to higher energy and has only a high energy tail, not a low energy one (not beyond that observed for the peak in coincidence with x rays), in accordance with what is expected if all, or most, of the ^{37}Cl had come from top of the ^{40}Ar.

Lastly, the very large difference between the Cl-Auger peak on top of ^{40}Ar [Fig. 6(a)] and the corresponding spectrum on top of Au [Fig. 6(b)] indicates that the environments of the recoiling Cl are very different in the two cases. If clumping were occurring each recoiling Cl ion would be closely surrounded by many ^{37}Ar atoms (for both substrates) and one would expect the Cl-Auger spectrum on Au to resemble the Cl-Auger spectrum on ^{40}Ar; clearly it does not.

Figure 10 shows the factors which affect the sensitivity of the recoil spectrum to the presence of a heavy neutrino peak, as a function of the heavy neutrino mass (bottom scale) and the corresponding recoil energy (top scale). The factors shown are those that apply to a spectrum measured in coincidences with x rays, for ^{37}Ar adsorbed on Au. Figure 10(a) shows the reduction in the detected fraction of ions due to increased neutralization as the recoil energy decreases, as obtained from the MC calculation. Note that the fraction is compared to that detected for recoils accompanying a zero-mass neutrino (recoil energy of 9.54 eV). Figure 10(b) shows the reduction in the yield due to the decrease in phase space which would accompany the emission of a heavy neutrino. Again, the plot compares the square of the momentum of a heavy neutrino $p^2(m_\nu)$ to that of a zero mass neutrino $p^2(0)$. Figure 10(c) shows the ratio of the width of the normal peak accompanying the emission of a zero-mass neutrino to that of the heavy neutrino. The increase in width is partially due to the increased interaction of the lower energy ion with the surface (at a lower velocity the Cl becomes ionized at a closer distance to the surface and hence experiences a larger image potential), and partly due to the technique of time of flight itself, which, for the same fractional energy spread, gives broader peaks for longer times of flight (lower speeds). The above three effects combine to give a peak height for a massive neutrino that is substantially reduced, compared to the peak height accompanying normal neutrino emission. Figure 10(d) shows the resulting height for a massive neutrino peak, compared to that of a zero-mass neutrino peak, assuming 100% mixing. For example, if a 600 keV neutrino were mixed completely with the electron neutrino, the height of the resulting low energy peak (4.3 eV) recorded in the time of flight spectrum would be only about 7% of the height of the zero mass peak at 9.54 eV.

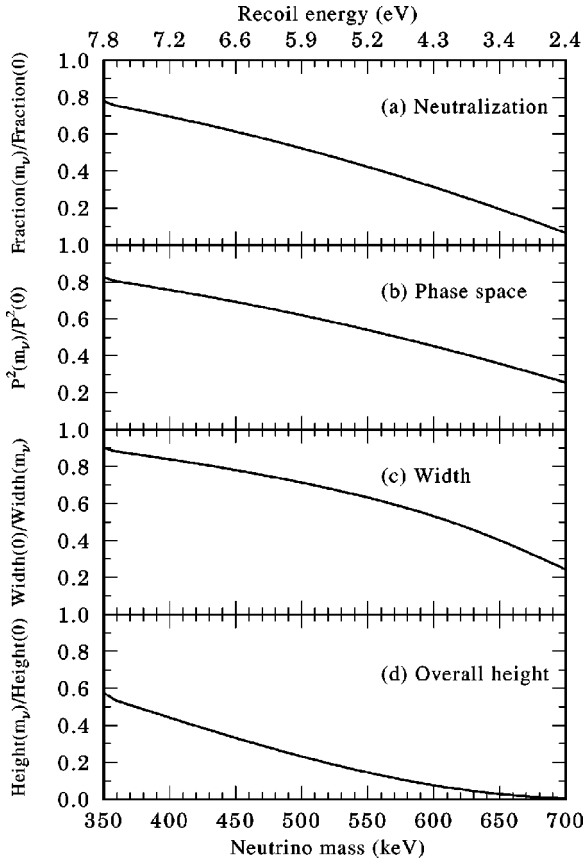

FIG. 10. Plots of various effects which reduce the sensitivity of the time of flight spectrum for ^{37}Ar adsorbed on gold and recorded in coincidence with x rays, to the presence of a heavy neutrino peak, as a function of the heavy neutrino mass. The top scale shows the corresponding recoil energy. (a) Decrease in detected fraction due to increase in neutralization, (b) decrease in phase space, (c) increase in peak width, (d) overall effect on peak height.

B. Fits and results

Three types of spectra were searched for massive neutrinos: with Au as a substrate, spectra obtained in coincidence with Auger electrons and with x rays were searched, and with ^{40}Ar as a substrate, only spectra in coincidence with x rays were searched. A sample of each of these is shown in

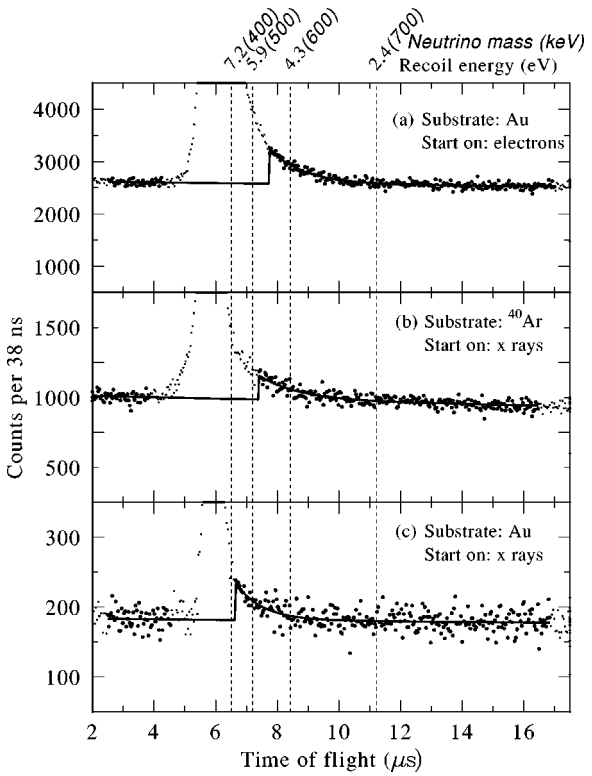

FIG. 11. Sample time of flight spectra showing the portion of the spectra (solid circles) used in the fit while searching for a heavy neutrino peak. (a) Spectrum recorded in coincidence with electrons with the ^{37}Ar adsorbed on gold, (b) spectrum recorded in coincidence with x rays with the ^{37}Ar adsorbed on top of ^{40}Ar, and (c) spectrum recorded in coincidence with x rays with the ^{37}Ar adsorbed on gold. The vertical dashed lines show the expected location of a peak due to the emission of a heavy neutrino with the indicated mass and recoil energy. The solid lines show the fit to the data (with no massive neutrino peak) using a linear term plus an exponential tail.

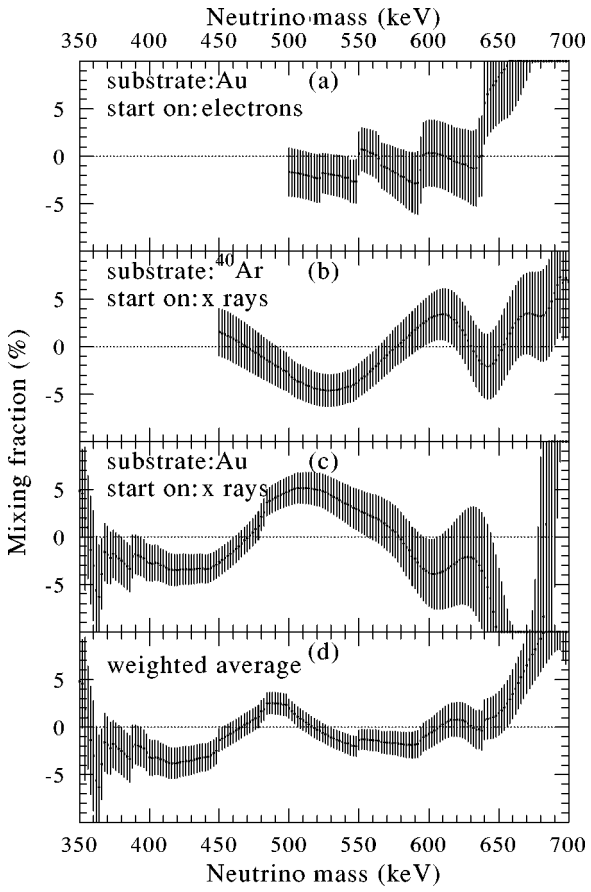

FIG. 12. Mixing fractions, as a function of heavy neutrino mass, extracted from fits to the spectra taken (a) in coincidence with electrons for ^{37}Ar adsorbed on gold, (b) in coincidence with x rays with the ^{37}Ar adsorbed on top of ^{40}Ar, and (c) in coincidence with x rays with the ^{37}Ar adsorbed on gold. (d) Weighted average mixing fractions.

Fig. 11. From each spectrum only the region indicated by the solid circles was included in the fit. That is, the main peak was not included, in order that it not drive the fit. The remaining part of the spectrum was fit with a linear term (to account, to first order, for accidental coincidences) plus an exponential which starts at some point on the low energy side of the main peak, to account for the tail of the peak:

$$N(t)=a_0+a_1t+\begin{cases} a_2\exp(-a_3t) & \text{if } t\geq t_0, \\ 0 & \text{if } t<t_0. \end{cases}$$

While there is no theoretical justification for using an exponential to describe the tail, the reasons it was used were (1) the resulting fits had reduced chi squareds that were all close to unity and (2) the monotonic nature of the exponential makes it difficult to simulate a peak, if it is not in the spectrum, or to suppress a peak that is present in the spectrum. For the heavy neutrino peak a Gaussian was used. For each massive neutrino peak, the width and position of the peak were fixed, using the results of the MC calculation discussed above, and the height was allowed to vary freely to minimize the chi squared. In addition to varying the height of the Gaussian, the four parameters describing the background (a_0–a_3) were also allowed to vary freely.

Figure 11 also shows the location expected for a massive neutrino peak with the indicated mass and recoil energy. From the spectra it is clear that the limitation on the sensitivity to ''low'' masses is the tail and width of the main peak. As shown in Fig. 11(c), the TOF spectra taken in coincidence with x rays with the Au substrate are the most sensitive, while the TOF spectra in coincidence with Auger electrons [Fig. 11(a)] are the least sensitive. The twelve spectra of the type shown in Fig. 11(a) were each searched for a massive neutrino peak, in steps of 2 keV in the neutrino mass. Similarly, the twelve spectra of the type shown in Fig. 11(c) and the four spectra of the type shown in Fig. 11(b) were also searched for massive neutrinos in 2 keV steps.

The extracted peak areas, converted to a mixing fraction by correcting for the phase space factor and the neutralization factor, from fits to spectra of the type shown in Figs. 11(a)–11(c), are shown in Figs. 12(a)–12(c), respectively. The results are the weighted average over all of the spectra of a given type. The error bars shown are 1σ errors. Some of the apparent discontinuities in the extracted fractions [most notable in Fig. 12(a)] are due to the fact that the starting time for the exponential term used in the fit is different for the different spectra (because of the above indicated variations in the widths and centroids) and hence not all analyzed spectra contribute to the average mixing fraction at all the neutrino

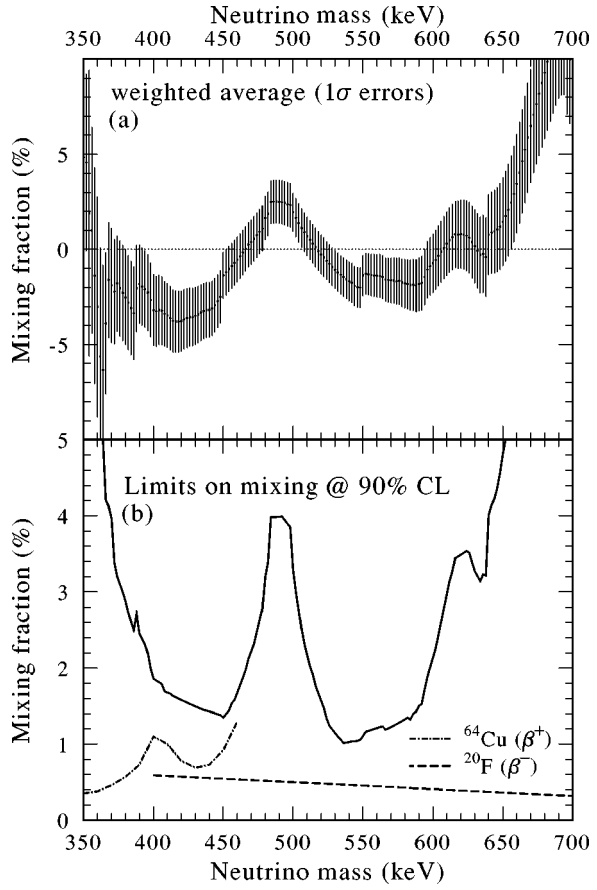

FIG. 13. (a) The weighted average fraction mixing for a heavy neutrino of the indicated mass extracted from fits to the time of flight spectra, and (b) the corresponding upper limits on the mixing fraction at the 90% confidence level. Also shown are the upper limits over the same mass region extracted from a search for kinks in the β^+ spectrum of ^{64}Cu (dash-dotted line) and from a search for kinks in the beta spectrum of ^{20}F (dashed line).

masses. Figure 12(d) shows the weighted average mixing fractions for all spectra types, at each neutrino mass. The peak (at the 2σ level) at a mass of 490 keV appears in only one type of spectrum [coincidences with x rays with the Au substrate, Fig. 12(c)], and not in the others. Therefore we discount the possibility that this is evidence for a heavy neutrino. One possible explanation for the enhancement in that particular spectrum at that energy is that this feature is a residual effect of recoils with charge $+2$ [Fig. 8(b)].

Figure 13(a) shows, again, the weighted average mixing fraction for all the data with 1σ error bars, and the resulting upper limits on the mixing fraction, at the 90% confidence level [Fig. 13(b)]. In obtaining the confidence level we have followed the recommendations of the Particle Data Group [31] for the treatment of Gaussian probability distributions in cases where the observable goes into an unphysical region (in this case the mixing fraction becoming negative).

Also shown in Fig. 13(b) are the upper limits, again at the 90% confidence level, from two searches that overlap the mass region investigated in the current work: (1) a search for kinks in the β^+ spectrum of ^{64}Cu [15] and (2) from a search for kinks in the β^- spectrum of ^{20}F [16]. While our upper limits are not lower than the existing limits, it should be pointed out that the limits from the β^- spectrum of ^{20}F apply, strictly speaking, to antineutrinos. Thus, in the mass region of $\approx$450–650 keV, the upper limits obtained in this work are the only directly measured limits, to our knowledge, on the admixture of the electron neutrino with the τ neutrino.

IV. CONCLUSIONS

While the lowest upper limit of $\approx$1% (at 550 keV) is about a factor of 2.5 higher than the corresponding limit for the antineutrino, it, nevertheless, is the lowest limit in this mass range on the admixture of the neutrino. Further, the result was obtained using an entirely different technique, so it does serve as a confirmation, at some level, of the antineutrino result, assuming CPT invariance. It is generally the case that nuclear physics limits on the mass of the neutrino are much higher than the corresponding limits on the antineutrino (225 eV for the mass of the electron neutrino [32], versus 5–10 eV for the mass of the electron antineutrino [4]).

We estimate the uncertainty in our quoted limits to be about 20%, owing to our use of Monte Carlo simulations to estimate the neutralizing fraction and the widths and energy shifts of the low energy recoils. One way to *measure* these quantities is to make use of coincidences with IB radiation that is emitted in about 10^{-4} of the EC decays. In IB decay three bodies share the momentum and energy: the neutrino, the recoiling atom, and the IB photon. If one were to detect, say, a 600 keV IB γ with a detector directly opposite to the recoil detector, one would observe two peaks in the TOF spectrum, one at an energy of 9.54 eV, corresponding to the case where the neutrino, with energy 214 keV, went in the same direction as the γ, and the other at an energy of 2.15 eV, corresponding to the case where the neutrino went in the opposite direction as the γ. By selecting the γ ray energy one can then select the energy of the second, low energy peak, and study the line shapes and fractions of these low energy recoils. Clearly, because of the low probability of IB, these would be very difficult and very time consuming measurements, but we are currently studying the feasibility of such measurements. We are also considering ways of improving the limits we obtained, both through obtaining more statistics, and through a better understanding of the energy distribution of the recoils, although it does seem to be difficult to lower the limit by more than a factor of 2. We are also considering the possibility of using other electron capturing isotopes, such as ^{7}Be. Although the latter has a much higher recoil energy than ^{37}Ar (57 eV vs 10 eV), the chemical activity of the ^{7}Be will introduce new complications, not encountered in the ^{37}Ar case.

Finally, we note that the narrowest width we obtained with our method (1.5 eV FWHM for one of the ion–x-ray coincidence spectra) is considerably smaller than the 2.7 eV obtained with a gaseous source for charge $+3$ [10] and slightly smaller than the 1.7 eV which is obtained for charge $+1$ ^{37}Cl with a gaseous ^{37}Ar source at room temperature [10]. So while it might be difficult to obtain much lower limits on the admixture of massive neutrinos from the recoil spectra of an adsorbed ^{37}Ar source, because that entails looking for very small peaks at low energy, the recoils from EC decay may be very useful as a source of quasi monoenergetic, low energy ions. These could be used to probe surface-

ion interactions and, if the source is covered with a few monolayers of some other species, to study the penetration of low energy recoils in thin films, a topic of current interest in solid state physics [33].

Note added in proof. After the submission of this article two works reporting evidence for neutrino oscillations have appeared. One reports $\nu_\mu \rightarrow \nu_e$ oscillations [34] and the other possibly $\nu_\mu \rightarrow \nu_\tau$ oscillations [35]. To our knowledge there is no inconsistency between our work and these works, since the neutrino mass range excluded by this work is much higher than that considered in these recent works.

ACKNOWLEDGMENTS

The assistance of Daniel Bardayan, Alex Altgilbers, Brian Faircloth, Anna Hagenston, and Cory Krum is gratefully acknowledged. The assistance of the staff of the Image and Chemical Analysis Laboratory at Montana State University is also gratefully acknowledged. The authors benefited from talks with Dr. Raymond Davis, Jr. on the preparation and cleaning of ^{37}Ar. This work was supported by the U.S. Department of Energy, Nuclear Physics Division, via Grant Nos. DE-FG05-87ER40314 and DE-FG02-96ER40955.

[1] W. Pauli (unpublished); reproduced in L. M. Brown, Phys. Today **31**(9), 23 (1978).
[2] F. Reines and C. L. Rowan, Phys. Rev. **90**, 492 (1953).
[3] See, for example, *Particle & Nuclear Astrophysics & Cosmology in the Next Millenium*, Proceedings of the 1994 Snowmass Summer Study, Snowmass, Colorado (World Scientific, Singapore, 1995), and references therein.
[4] Particle Data Group, R. M. Barnett *et al.*, Phys. Rev. D **54**, 1 (1996).
[5] G. Barenboim and M. Raidal, Phys. Lett. B **406**, 219 (1997), and references therein.
[6] B. Saraf, Phys. Rev. **102**, 466 (1956); recalculated by Bambynek *et al.*, Rev. Mod. Phys. **49**, 77 (1977).
[7] *Table of Isotopes*, 8th ed., edited by R. B. Firestone and V. S. Shirley (Wiley, New York, 1996).
[8] G. W. Rodeback and J. S. Allen, Phys. Rev. **86**, 446 (1952).
[9] O. Kofoed-Hansen, Phys. Rev. **96**, 1045 (1954).
[10] A. H. Snell and F. Pleasonton, Phys. Rev. **86**, 446 (1955).
[11] J. S. Allen, Phys. Rev. **61**, 692 (1942).
[12] P. B. Smith and J. S. Allen, Phys. Rev. **81**, 381 (1951).
[13] R. Davis, Jr., Phys. Rev. **86**, 976 (1952).
[14] J. P. Deutsch, M. Lebrun, and R. Prieels, Phys. Rev. D **27**, 1644 (1983).
[15] K. Schreckenbach, G. Colvin, and F. von Feilitzsch, Phys. Lett. **129B**, 265 (1983).
[16] J. Deutsch, M. Lebrun, and R. Prieels, Nucl. Phys. **A581**, 149 (1990).
[17] E. Glikman, I. Kelson, and N. V. Doan, J. Vac. Sci. Technol. A **9**, 2776 (1991).
[18] M. M. Hindi, Lin Zhu, Recep Avci, P. M. Miočinović, R. L. Kozub, and G. J. Lapeyre, Phys. Rev. A **53**, R3716 (1996).
[19] B. Brehm, J. Grosser, T. Ruscheinski, and M. Zimmer, Meas. Sci. Technol. **6**, 953 (1995).
[20] J. C. Levin, C. Biedermann, N. Keller, L. Liljeby, C.-S. O, R. T. Short, I. A. Sellin, and D. W. Lindle, Phys. Rev. Lett. **65**, 988 (1990); D. W. Lindle, W. Les Manner, L. Steinbeck, E. Villalobos, J. C. Leven, and I. A. Sellin, J. Electron Spectrosc. Relat. Phenom. **67**, 373 (1994).
[21] R. Hentschke, K. J. Snowdon, P. Hertel, and W. Heiland, Surf. Sci. **173**, 565 (1986).
[22] H. D. Hagstrum, Phys. Rev. **96**, 226 (1954).
[23] P. M. Echenique, R. H. Ritchie, N. Barberán, and J. Inkson, Phys. Rev. B **23**, 6486 (1981).
[24] J. Burgdörfer, P. Lerner, and F. W. Meyer, Phys. Rev. A **44**, 5674 (1991).
[25] C. Kittel, *Introduction to Solid State Physics*, 6th ed. (Wiley, New York, 1986).
[26] M. O. Krause, J. Phys. Chem. Ref. Data **8**, 307 (1979).
[27] M. O. Krause and J. H. Oliver, J. Phys. Chem. Ref. Data **8**, 329 (1979).
[28] M. H. Chen, B. Crasemann, and H. Mark, At. Data Nucl. Data Tables **24**, 1 (1979).
[29] D. M. Young and A. D. Crowell, *Physical Adsorption of Gases* (Butterworths, London, 1962), p. 20.
[30] T. M. Miller, in *CRC Handbook of Chemistry and Physics*, 73rd ed., edited by P. R. Lide (CRC Press, Boca Raton, 1992), Secs. 10-180–10-213.
[31] Review of Particle Properties, Phys. Lett. B **239**, 1 (1990).
[32] P. T. Springer, C. L. Bennet, and P. A. Baisden, Phys. Rev. A **35**, 679 (1987).
[33] Norbert J. Sack, Mustafa Akbulut, and Theodore E. Madey, Phys. Rev. Lett. **73**, 794 (1994).
[34] C. Athnassopoulos *et al.*, Phys. Rev. Lett. **81**, 1774 (1998).
[35] Y. Fukuda *et al.*, Phys. Rev. Lett. **81**, 1562 (1998).
[36] C. Athanassopoulos *et al.*, Phys. Rev. Lett. **77**, 3082 (1996).
[37] J. E. Hill, Phys. Rev. Lett. **75**, 2654 (1995).
[38] R. W. Kiser and W. H. Johnston, J. Am. Chem. Soc. **81**, 1810 (1959).
[39] From *CRC Handbook of Chemistry and Physics*, edited by Robert C. Weast (CRC Press, Boca Raton, FL, 1990), p. E-70.